PHYSICAL REVIEW D **86,** 075018 (2012)

Model independent reach for W' bosons at the LHC

Daniel Duffty* and Zack Sullivan†

Department of Physics, Illinois Institute of Technology, Chicago, Illinois 60616-3793, USA

(Received 23 August 2012; published 16 October 2012)

The semileptonic decay of single-top-quark production provides a strong probe for W' bosons at the CERN Large Hadron Collider. We propose an explicit search strategy for $pp \to W' \to tb \to l\nu bj$ for use at 7 and 8 TeV collider energies and integrated luminosities ranging from 5 to 20 fb^{-1}. Based on detector-simulated results, we predict that a lower bound can be placed on the mass of right-handed W'_R with standard model-like couplings of $m_{W'_R} > 1800$ GeV at $\sqrt{S} = 7$ TeV with 5 fb^{-1} and of $m_{W'_R} > 2000$ GeV at 8 TeV with 20 fb^{-1}. For left-handed W'_L bosons, we find a lower bound of 1750–1800 GeV at 7 TeV and 5 fb^{-1}, depending on the sign of the interference with standard model single-top-quark production. We present effective coupling g'-dependent limits for accessible masses and stress the importance of these limits for comparison with theoretical models.

DOI: 10.1103/PhysRevD.86.075018 PACS numbers: 14.70.Pw, 14.65.Ha, 12.60.Cn, 13.85.Rm

I. INTRODUCTION

The search for new charged vector currents, generally called W' bosons, plays an important role in many extensions of the standard model. Some theories propose higher mass W boson resonances [1]; while others propose right-handed counterparts to the left-handed standard model W in a broken $SU(2)_L \times SU(2)_R$ symmetry [2–5]. Still others propose a heavy mass eigenstate in strongly interacting theories, such as noncommuting extended technicolor [6]. All of the W' bosons in these theories enter the Lagrangian with terms of the form

$$\mathcal{L} = \frac{g'}{2\sqrt{2}} V'_{ij} W'_\mu \bar{f}^i \gamma^\mu (1 \pm \gamma_5) f^j + \text{H.c.}, \qquad (1)$$

which mirrors that of the standard model W (without the lepton sector if it is right-handed). While there could be left-right mixing, such mixing is constrained by K-$\bar{K}$ mixing [7]; hence, theories have been proposed that would suppress this naturally via orbifold breaking of the left-right symmetry [8] or supersymmetric interactions [9].

While the phenomenology of models beyond the standard model (SM) is generally complex, it was demonstrated in Ref. [10] that W' sectors can be factorized through next-to-leading order (NLO) in QCD into terms of the form of Eq. (1). Hence, it was proposed that searches for direct resonances decaying into a tb final state be used to bound all such possible models that couple to quarks. Following Ref. [10], a series of searches was performed by the CDF [11,12], and D0 [13,14] Collaborations at the Fermilab Tevatron, setting the world's strongest bounds on right-handed W' bosons and competitive bounds on left-handed W' bosons [15].

Recent interest by the ATLAS and CMS Collaborations in extending these studies to the CERN Large Hadron Collider (LHC) has prompted a reexamination of the reach and interpretation of these models. Early results by ATLAS [16] and CMS [17] utilize NLO cross sections from an early draft of this paper (reproduced here in the Appendix). In Sec. III, we compare our predictions with these first results.

In this paper we extend earlier predictions for the model-independent reach for W' bosons at a 14 TeV LHC [18] to 7 and 8 TeV energies. In Sec. II, we provide details of our detector simulation. We point out previously undescribed kinematic differences between right- and left-handed W' bosons ($W'_{R,L}$) that play a role in the reach at the LHC. In addition, we examine the effect of W' charge on the distributions at a pp collider. In Sec. III, we propose a set of cuts for the model-independent analysis and describe our predictions for the reach at the LHC for 7 and 8 TeV. We conclude with suggestions for further research. In the Appendix, we provide updated predictions for NLO W' cross sections for 7 and 8 TeV pp colliders, including all theoretical uncertainties, for use by the coming experimental analyses.

II. SIMULATION

The signal of interest is $pp \to W' \to tb$, where the top quark decays as $t \to Wb$, and the W decays leptonically to an electron or muon plus a neutrino. In order to simulate the full decay chain, including all angular correlations, we utilize a general W' model [19] in MADEVENT [20] to produce parton-level signal and background events. These events are fed through PYTHIA [21] to generate initial- and final-state showering and reconstructed in an ATLAS-like detector model in a modified PGS-4 [22] detector simulation.

We add an anti-K_T jet reconstruction algorithm to PGS in order to match the current jet algorithms used by the ATLAS and CMS Collaborations. We use a cone size of 0.4 for the anti-K_T cutoff and apply a jet energy scale

*dduffty@IIT.edu
†Zack.Sullivan@IIT.edu

correction to recover energy lost due to detector resolution and limited cone size. This jet energy scale correction is extracted from identified b jets in a $Zb \to e^+e^-b$ test sample. The resulting correction is small for jet energies grater than $\sim$50 GeV and is implemented by scaling the jet four-momentum as

$$p'_\mu = p_\mu\left(1 + \frac{2.2}{E} + \frac{62.2}{E^2}\right). \quad (2)$$

After the jet energy correction is applied, we find very little dependence in the final results on cone sizes between 0.4 and 0.7.

An important feature in reducing backgrounds to the tb final state is the use of b-tagging. We model b-tagging with the default PGS tight-tagging algorithm, modified to include muon tracks inside of a jet. For the cuts we employ below this leads to $\sim$50% b-tagging efficiency, with a somewhat overestimated $\sim$2% mistag rate for light quarks and a charm mistag rate of $\sim$10%. The effect of other b-tagging scenarios is addressed in Sec. III.

Since our interest is in W' bosons with masses near or above 1 TeV, we expect the b jet that recoils against the top quark in the event to have a transverse energy $E_T \sim$ 500–1200 GeV. At this stage it is unclear what the ultimate b-tagging efficiency will be for these high-energy jets; however, we expect the decay products of the B hadrons to be so boosted that secondary vertex reconstruction will be difficult. For the purposes of this study, we assume that we are unable to make use of b-tagging for the leading jet in our events. Should an algorithm for high efficiency and high purity b jets near 1 TeV be developed, it could improve the signal purity.

The primary backgrounds of this W'-induced s-channel single-top-quark process will be t-channel single-top-quark production, $t\bar{t}$ decaying to a lepton plus jets, and Wjj production. t-channel single-top-quark production is significant because the lead jet and the top quark will have a large invariant mass due to the large angular separation between decay products. Wjj is a major background strictly because its large cross section compensates for its small light jet mistag rate. Other important backgrounds are the dilepton decay channel of $t\bar{t}$, where one of the leptons is lost within a jet, other W + jet events (Wcj, Wcc, Wbj, Wbb), and standard model s-channel single-top-quark production.

Background events are reweighted to match their NLO cross sections using a scale of 1 TeV calculated using Monte Carlo for FeMtobarn processes (MCFM) [23] after acceptance cuts and CTEQ 6.6 parton distribution functions (PDFs) [24]. The s- and t-channel single-top-quark normalizations are confirmed with matching to ZTOP [25]. Normalizing the W' signal to NLO is somewhat more subtle. Here, we use the code from Ref. [10] updated for 7 and 8 TeV pp colliders (see the Appendix for inclusive cross sections with theoretical errors).

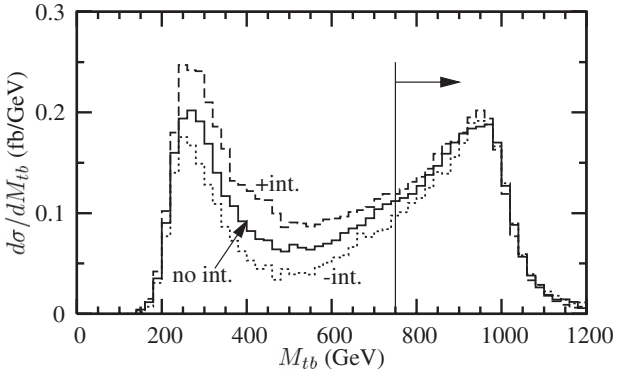

FIG. 1. Reconstructed invariant mass M_{tb} for a 1 TeV SM-like left-handed W' boson and standard model $pp \to W \to tb$ s-channel production processes. These processes can be non-interfering, constructively interfering (+ int.), or destructively interfering (− int.), but at the large invariant mass relevant for discovery, the interference is small.

The normalization for right-handed W'_R bosons is straightforward, but left-handed W'_L bosons can interfere with standard model W-propagated single-top-quark production. As pointed out in Ref. [19], the W'-W interference can be constructive, destructive, or negligible, depending on the sign and size of the V'_{tb} term in the W' mixing matrix with respect to the other elements; a positive term (as is usually assumed [26]) in the mixing matrix yields a destructive interference, while a negative term in the mixing matrix provides a constructive interference. We consider the two limiting cases of fully destructive and constructive interference below in order to bound the range of possible results.

To fix the NLO normalization for left-handed W'_L bosons, we extract a K factor after cuts from the case of no interference and scale up or down the events in the interfering cases by the same K factor. We justify and quantify the error in this approximation as follows: First, we observe in Fig. 1 that for maximal SM-like coupling ($g'/g_{\rm SM} = 1$), the interference can be large in certain regions of reconstructed invariant mass of the tb. Fortunately, we are only interested in large invariant masses—close to the W' boson mass—where the interference is never more than $\sim$20%. The K factor itself is typically $\sim$1.2 for the masses we consider. Furthermore, both standard model single-top-quark production and W'_L production have identically factorizable matrix amplitudes [10] at NLO. Hence, they receive the same QCD corrections at NLO. Put together, we estimate the maximum error we introduce by using leading-order interference and normalizing in this fashion is $\sim 0.2 \times 0.2$ or 4%. This error is negligible when compared with the 10–30% error introduced by parton distribution function uncertainties (listed in the Appendix).

A. Kinematic features

The inclusive cross sections for right- and left-handed W' bosons decaying to tb differ mostly in their branching

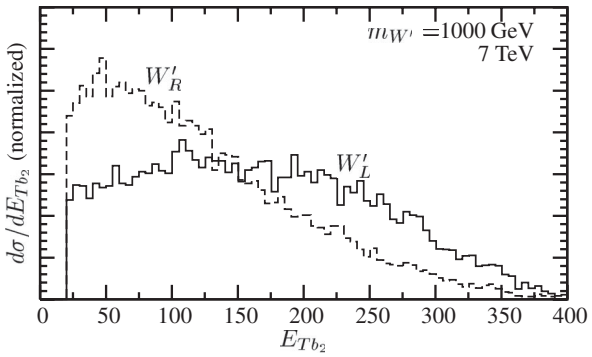

FIG. 2. Normalized transverse energy distribution of the second b jet E_{Tb_2} for W'_R and W'_L bosons with a mass of 1 TeV.

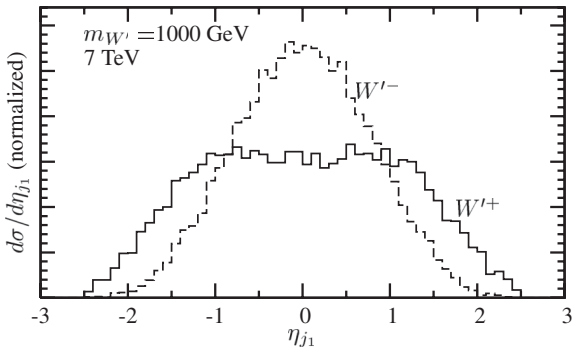

FIG. 4. Normalized pseudorapidity distribution of the leading jet in W'^+_R and W'^-_R decays for a W' mass of 1 TeV.

fractions. Since there are no light right-handed neutrinos, we expect roughly $4/3$ as many tb from W'_R decay as from W'_L decay. The larger branching fraction suggests there will be a slightly better reach for right-handed bosons than left-handed bosons. This is true, but there are kinematic differences between right- and left-handed bosons, as well as between W'^+ and W'^- bosons, that affect the acceptances and reconstruction efficiencies.

Spin correlations, usually considered as a way to distinguish right-handed from left-handed W' bosons, also modify the distributions of jets and leptons in the detector. The dominant parton luminosity for W' boson production involves a valence-sea quark combination, $u\bar{d}$ or $d\bar{u}$. On average this leads to a forward boost of the W' bosons and their decay products in the direction of the valence quark. Spin correlations between the down-type parton in the initial state and the b jet from the top quark decay, or the d and the charged lepton from the W decay, affect right- and left-handed W' bosons differently.

Bottom jets from the top quark in W'_R decay are partially antialigned with the W'_R direction, leading to a slightly softer transverse energy E_{Tb} spectrum than for W'_L bosons. In Fig. 2, we see this softer E_{Tb} spectrum for 1 TeV W'_R vs W'_L bosons. This feature reduces our final prediction of the reach for right-handed W' bosons at lower masses, as a large fraction of events fail to pass minimal jet acceptance cuts. Lepton acceptance is also reduced for W'_R bosons, as the spin correlations make them more forward; though we see in Fig. 3 the effect is small.

More striking than left-right differences are the differences between W'^+ and W'^- bosons. The cross section for W'^+ is roughly twice that of W'^-, since there are roughly twice as many valence u quarks as valence d quarks in the proton. The spin correlations exaggerate the effect to produce very different rapidity distributions for the final state particles. The leading jet in the W'^- decay is more central in pseudorapidity η_{j_1} than in W'^+ decay, as shown in Fig. 4 for right-handed W' bosons. Fortunately, detector acceptance at the LHC covers the entire rapidity range for both. The lepton pseudorapidity η_l in Fig. 5, however, is more forward for W'^+ than for W'^-. This will lead to a slightly different detector response between the two production modes. In this analysis, we sum over both W'^+ and W'^- production with the same cuts, but future studies might consider optimizing cuts for W'^+ and W'^- analyses separately.

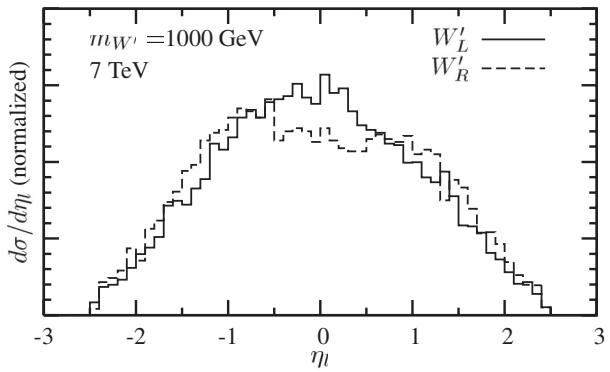

FIG. 3. Normalized lepton pseudorapidity η_l for W'_R and W'_L bosons with a mass of 1 TeV.

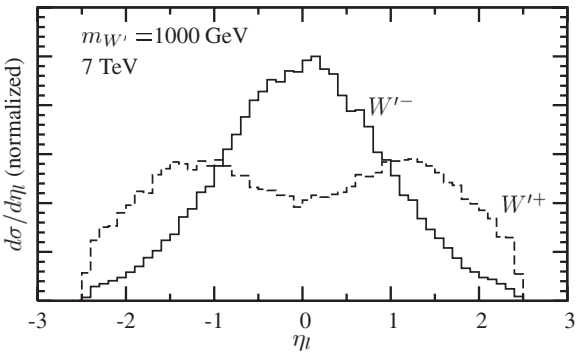

FIG. 5. Normalized pseudorapidity distribution of the charged lepton in W'^+_R and W'^-_R decays for a W' mass of 1 TeV.

III. RESULTS

We propose a simple cut-based search for W' bosons that is effective at 7 and 8 TeV energies at the LHC. While we saw in Sec. II several strong angular correlations that affect acceptances, we find that the ultimate significance of a W' signal in the presence of backgrounds is dominated by purely kinematic effects. Hence, we make use of those distinctive kinematic features here.

In this analysis we are examining the $pp \to W' \to tb \to l\nu bj$ final state, where l is an electron or muon. Since all of our signal events are fairly central, we begin with a basic set of detector acceptance cuts that require at least two jets with $E_{Tj} > 20$ GeV and $|\eta_j| < 2.5$, one lepton with $p_{Tl} > 20$ GeV and $|\eta_l| < 2.5$, and missing transverse energy $\not{E}_T > 20$ GeV. (All cuts are summarized in Table I.) At the level of acceptance cuts, the signal-to-background ratio $S/B \sim 1/1000$ for a canonical right-handed W' boson with standard model-like couplings ($g'/g_{\rm SM} = 1$).

The most distinctive feature of these W' bosons is the highly energetic leading bottom jet. As mentioned above, we avoid attempting to b-tag this jet and instead simply require it to have a transverse energy $E_{Tj_1} > 0.2 m_{W'}$. This cut has a minimal effect on the signal, since the leading jet has energies approaching $0.5 m_{W'}$ (up to detector resolution). However, all backgrounds have a leading jet E_T that is falling with energy for the masses we consider. As we see in Table II, after this cut S/B improves to $1/20$ for a 1 TeV SM-like W'_R. The dominant background is due to mistags from Wjj, but this is reducible.

The next most distinctive element of the signal is the b jet coming from the top quark decay. This jet is often, but not always, the second-hardest jet in the event. Sometimes showered jets accidentally have a larger energy, and sometimes the jet that recoils against the top quark is reconstructed at lower energy. In order to capture most of the signal events, we require at least one b-tagged jet that is *not* the leading jet in the event. If there are more than one b-tagged jet, we assume the highest E_T b jet is the one coming from the top quark decay. The main effect of this cut is to reduce the Wjj-oriented backgrounds (Wjj, Wcj, and Wcc) by a factor of 20, improving S/B to roughly $1/3.5$ for a SM-like W'_R.

TABLE I. Acceptance and analysis cuts for $pp \to W' \to tb \to l\nu bj$.

Lead jet	$E_{Tj_1} > 0.2 m_{W'}$	$\lvert\eta_{j_1}\rvert < 2.5$
b-tagged jet	$E_{Tb} > 20$ GeV	$\lvert\eta_b\rvert < 2.5$
Leading $e^\pm$ or $\mu^\pm$	$p_{Tl_1} > 20$ GeV	$\lvert\eta_{l_1}\rvert < 2.5$
Second $e^\pm$ or $\mu^\pm$	$p_{Tl_2} < 10$ GeV; or	$\lvert\eta_{l_2}\rvert > 2.5$
Missing E_T	$\not{E}_T > 20$ GeV	
Reconstructed top	$M_{l\nu b} < 200$ GeV	
W' mass window	$0.75 m_{W'} < M_{l\nu bj} < 1.1 m_{W'}$	

TABLE II. Cross sections (fb) for signal and backgrounds at each level of cuts, assuming a 1 TeV right-handed W' boson with standard model-like couplings ($g'/g_{\rm SM} = 1$) at a 7 TeV LHC.

Process	$jjl\not{E}_T$	E_{Tj_1} cut	b tag	$M_{l\nu b}$	$M_{l\nu bj}$
Wjj, Wcc, Wcj	219 000	5680	230	83.8	12.9
Wbb, Wbj	2580	42.3	16.4	6.4	0.8
$t\bar{t}$	8010	136	70.2	40.3	8.4
t-chan. single top	1590	61.3	30.1	23.8	6.8
s-chan. single top	182	8.5	3.6	2.7	0.4
Background total	231 000	5830	350	157	29.3
W' signal	294	247	106	79.8	76.3

The relative sizes of the Wjj, t-channel single-top-quark and $t\bar{t}$ backgrounds are highly affected by the choice of b-tagging efficiencies. A large b acceptance rate would allow a greater acceptance of signal events but would have a relatively larger proportion of Wjj events. For example, a 70% b acceptance is achievable [27] and would increase the signal and background top-quark final states' acceptance by about 40%, but the Wjj backgrounds would increase by more than a factor of 2 with current algorithms. The net effect would be a lower signal purity, and no gain in significance.

For this analysis we choose to improve the signal purity by roughly reconstructing a top-quark mass out of the b-tagged jet, the lepton, and the missing energy. We first reconstruct the W in top decay by assuming the W is on-shell and choosing the smallest rapidity solution for the neutrino four-momentum. In order to suppress sensitivity to the jet energy resolution, we place a mild upper cut on the $l\nu b$ invariant mass of $M_{l\nu b} < 200$ GeV. By choosing to ignore b tags of the leading jet, this cut reduces the $t\bar{t}$ background, as there is a 50% chance of tagging the b jet that is not associated with the leptonic final state. This cut is useful in obtaining the strongest limit on the $W'q\bar{q}$

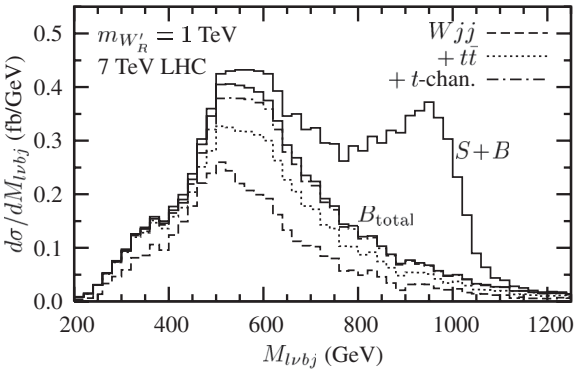

FIG. 6. Differential cross section in the reconstructed invariant mass $M_{l\nu bj}$ for the signal S and backgrounds, for a SM-like right-handed W'_R boson of mass of 1 TeV after acceptance cuts. The total background B is composed mostly of Wjj, $t\bar{t}$, and t-channel single-top-quark production.

TABLE III. Predicted reach in effective couplings ($g'/g_{\rm SM}$) for 95% C.L. exclusion of right- and left-handed W' bosons at $\sqrt{S} =$ 7 TeV in 5 fb^{-1} of data. Positive (+ int.) and negative (− int.) interference limits for W'_L are listed separately.

W' mass (TeV)	Right	Left (+ int.)	Left (− int.)
0.50	0.16	0.20	0.21
0.75	0.20	0.26	0.27
1.00	0.26	0.30	0.33
1.25	0.44	0.51	0.58
1.50	0.65	0.72	0.84
1.75	0.89	0.85	1.04
2.00	1.84	1.76	2.24
2.25	3.20	3.29	3.68
2.50	5.99	5.96	6.67
2.75	11.59	10.58	11.83
3.00	22.15	16.43	23.12

coupling g', but we explain in the Conclusions why this cut might be removed for more general studies.

After the cuts considered so far, a 1 TeV right-handed W' boson with SM-like couplings would have a very strong signature at the LHC. In Fig. 6, we see the cross section as a function of $M_{l\nu bj}$ invariant mass for the signal plus background compared to the steeply falling background. The background under the W' mass peak is composed of nearly equal parts t-channel single-top-quark production, $t\bar{t}$, and Wjj. In this analysis we consider W' masses from 500 GeV to 3.5 TeV and find that most of the signal events tend to fall in a mass window of $0.75m_{W'} < M_{l\nu bj} < 1.1m_{W'}$. When this cut is applied to the 1 TeV SM-like W'_R of Table II, we see that S/B improves from 1/2 to nearly 2.6/1, and the significance for discovery ($S/\sqrt{S+B}$) is greater than 16

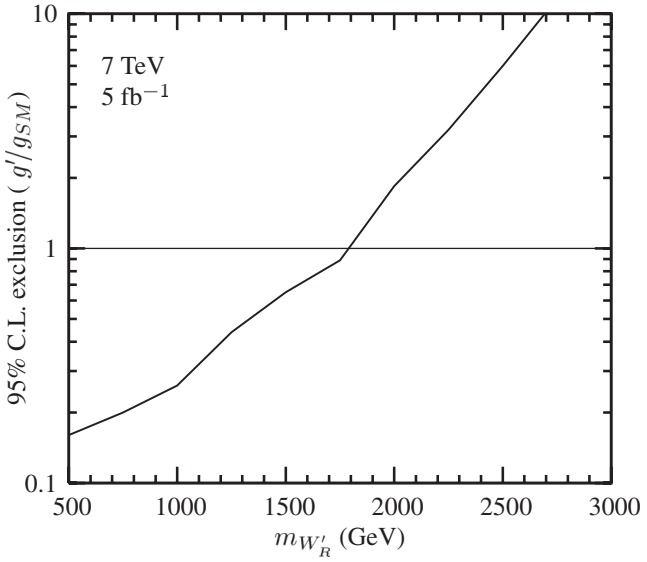

FIG. 7. Expected 95% C.L. exclusion limit for $g'/g_{\rm SM}$ for a right-handed W'_R boson at $\sqrt{S} = 7$ TeV and 5 fb^{-1} of data.

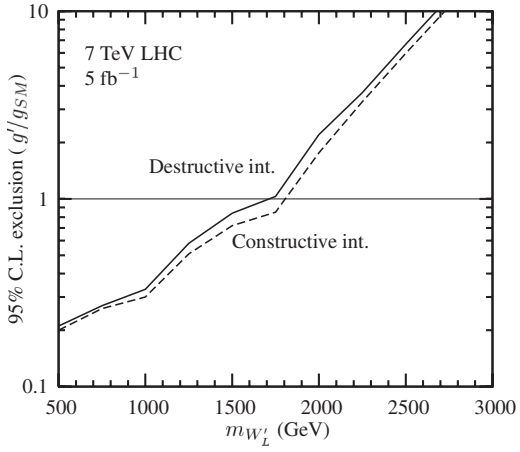

FIG. 8. Expected 95% C.L. exclusion limit for $g'/g_{\rm SM}$ for a left-handed W'_L boson at $\sqrt{S} = 7$ TeV and 5 fb^{-1} of data that interferes constructively or destructively with standard model single-top-quark production.

with 5 fb^{-1} of integrated luminosity at 7 TeV. This particular W' has already been excluded by early LHC data [16,17], but we use these cuts to answer what is the reach in effective coupling $g'/g_{\rm SM}$ vs W' boson mass.

In Table III, we list the 95% confidence level (C.L.) exclusion reach in effective coupling $g'/g_{\rm SM}$ with 5 fb^{-1} of integrated luminosity for masses between 500 and 3000 GeV at 7 TeV. This ratio is most useful for direct comparison to theoretical models with Lagrangians of the form in Eq. (1) [10,18,19]. For right-handed W'_R searches, the reach is approximately $\sqrt{4/3}$ times better than for left-handed W'_L due to the larger branching fraction for $W'_R \to tb$. As can be seen in Figs. 7 and 8, W' bosons can be excluded for $g'/g_{\rm SM}$ down to a few times 10^{-1} below 1.5 TeV. This is significantly smaller than the g' that appear in the models described in Sec. I. For standard model-like W' bosons, a limit could be set around 1.7–1.8 TeV, depending on

TABLE IV. Predicted reach in effective couplings ($g'/g_{\rm SM}$) for 95% C.L. exclusion of right- and left-handed W' bosons at $\sqrt{S} = 8$ TeV in 5 fb^{-1} of data. Positive (+ int.) and negative (− int.) interference limits for W'_L are listed separately.

W' mass (TeV)	Right	Left (+ int.)	Left (− int.)
0.50	0.17	0.21	0.21
0.75	0.26	0.30	0.31
1.00	0.35	0.38	0.42
1.25	0.51	0.53	0.60
1.50	0.70	0.70	0.81
1.75	1.06	0.99	1.20
2.00	1.59	1.41	1.75
2.25	2.44	2.05	2.63
2.50	3.79	3.11	4.11
2.75	6.19	4.75	6.47
3.00	10.29	7.71	10.84

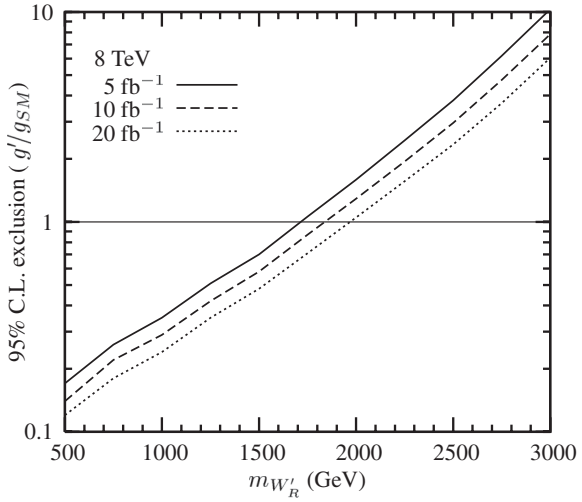

FIG. 9. Expected 95% C.L. exclusion limit for g'/g_{SM} for a right-handed W'_R boson at $\sqrt{S} = 8$ TeV, with 5, 10, or 20 fb^{-1} of data.

handedness and the sign of interference. Note that the difference between constructive and destructive interference is only about a $\sim$10% effect on the final limit at any given mass. It is also important for experiments to demonstrate the exclusion for models with $g'/g_{\mathrm{SM}} > 1$, as models remain perturbative up to a ratio of about 5. For example, Kaluza-Klein models can have ratios of $\sqrt{2}$ or 2 [8].

In moving to 8 TeV at the LHC, we expect a slightly improved mass reach for SM-like W' bosons due to the additional available energy and improved reach in g'/g_{SM} from the increased signal cross section. However, we see in Table IV and Figs. 9 and 10 that at 5 fb^{-1} integrated luminosity, the reach is actually slightly worse than at

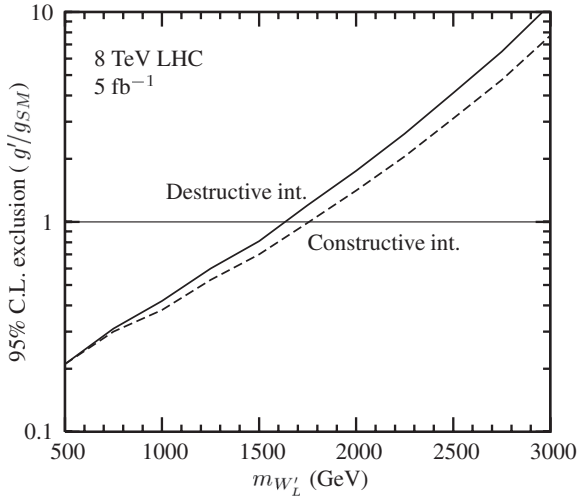

FIG. 10. Expected 95% C.L. exclusion limit for g'/g_{SM} for a left-handed W'_L boson at $\sqrt{S} = 8$ TeV and 5 fb^{-1} of data that interferes constructively or destructively with standard model single-top-quark production.

7 TeV. In general, the search below 2 TeV becomes more difficult because the gluon-initiated backgrounds (Wjj and $t\bar{t}$) grow faster with collider energy than the quark-initiated signal. In addition, the acceptance of the right-handed W'_R is reduced when compared to left-handed W'_L due to the kinematic distributions discussed in Sec. A. The greatest improvement in searches at the 8 TeV LHC comes for masses above 2 TeV and with the accumulation of additional data. In general, the limit on g'/g_{SM} improves roughly as the fourth root of the integrated luminosity ($L^{1/4}$). Hence, the LHC will improve upon limits from 7 TeV once the full data sample is accumulated.

The reach we predict with the cuts shown here represents an improvement over the similar ATLAS W' analysis of Ref. [16], which uses fixed cuts for all masses. This is due to the fact that as the W' mass increases, the lead jet cut is the most effective cut in removing background contamination. Our results are similar to the CMS analysis in Ref. [17], although we stress the coupling dependence as being critical for comparison with theory. The top mass cut coupled with our scaling leading jet cut has the potential to improve on the current CMS results by eliminating a large portion of the Wjj background and a significant portion of the $t\bar{t}$ background.

IV. CONCLUSIONS

In this paper, we investigate the reach in mass and coupling for arbitrary W' boson models where the W' decays to tb. For purely right-handed W'_R bosons, the 7 TeV run of the LHC could exclude standard model-like ($g'_R = g_{\mathrm{SM}}$) bosons of mass up to 1800 GeV with 5 fb^{-1} of integrated luminosity. Larger backgrounds at 8 TeV lead to a lower reach of 1700 GeV with 5 fb^{-1} of data, but a combined analysis of 20 fb^{-1} may exclude up to 1950 GeV. For left-handed W'_L bosons, a reach of 1750–1900 GeV is possible with 5 fb^{-1} depending on the sign of interference with standard model single-top-quark production. With a combined run of 20 fb^{-1} at 8 TeV, exclusions of 1900–2050 GeV are possible, with the highest exclusion when the W'_L interacts constructively with the standard model W boson.

In addition to W' mass reach for standard model-like couplings, we demonstrate the reach as a function of relative effective coupling g'/g_{SM}. We find that for masses near 1 TeV, 95% C.L. exclusion limits can be set around $g'/g_{\mathrm{SM}} \sim 0.2$–$0.3$. In addition, near 2.5 TeV, limits can be set on couplings below 3. These coupling-dependent limits are important, because they cover a large range of perturbative models. For example, in models where there are mixtures of multiple $SU(2)_L$, there are constraints on their couplings due to the measurement of g_{SM}:

$$\frac{1}{g_1^2} + \frac{1}{g_2^2} + \cdots + \frac{1}{g_n^2} = \frac{1}{g_{\mathrm{SM}}^2} \approx \frac{1}{0.427}. \qquad (3)$$

This implies $1.02 g_{\mathrm{SM}} < g_{1,2,\ldots} < \sqrt{4\pi}$ in these perturbative models. Hence, there will always be at least one W' boson with $0.187 < g'/g_{\mathrm{SM}} < 5.34$ [18]. While many theoretical models have a preference for $g'/g_{\mathrm{SM}} \sim 1$, the coupling-dependent limit catches most of them.

In some models the W' boson might decay through other recognizable channels with the same final state, e.g., $W' \to WZ \to Wb\bar{b}$ or $W' \to WH \to Wb\bar{b}$. These channels would both be detectable and have similar backgrounds to the single-top signal, but some of the cuts used in the analysis would no longer apply. Instead of a loose cut on the top-quark mass and a large leading jet E_T requirement, a relatively tight cut could be placed on the two jets to reconstruct the Higgs [28,29] or Z boson mass. Even a relaxation of the loose top-mass cut would allow enough access to these channels to say something about many of the models listed in Sec. I.

If a W' boson is discovered using these methods, the next logical step would be to establish its chirality. This can be accomplished by looking at the angular correlations between the charged lepton and the initial-state down quark in the reference frame of the top quark [10]. At the LHC this corresponds to a broadening of the pseudorapidity distribution of the lepton. Other kinematic variables shown in Sec. A may also be used.

While this paper discusses exclusion, the reach for discovery of a W' boson scales like $(g')^2$—i.e., the discovery reach curves are 1.6× the exclusion curves of Figs. 7–10. Hence, the model-independent search for W' bosons presented here has the potential to explore the parameter space of most charged vector current models that have been proposed within the past few years.

ACKNOWLEDGMENTS

This work is supported by the U.S. Department of Energy under Contract No. DE-SC0008347.

APPENDIX

We summarize here the inclusive cross sections plus theoretical uncertainties for the single-top-quark final state of W' production at the Large Hadron Collider. Cross sections are calculated for $t\bar{b}$ and $\bar{t}b$ separately, for both 7 and 8 TeV pp colliders. Cross sections at 7 TeV for right-handed W'_R bosons are listed by mass at leading order and NLO in femtobarns in Table V; and left-handed W'_L bosons are listed by mass at leading order and NLO in femtobarns in Table VI. Note, the left-handed cross sections assume *no interference* with the standard model production process. See Sec. II for a description of how we use the left-handed normalization. Cross sections at 8 TeV are listed for W'_R and W'_L in Tables VII and VIII, respectively.

Uncertainties in the Tables are listed in femtobarns at NLO. The cross section uncertainties are completely dominated by the errors in the CTEQ 6.6 PDFs [24] and are calculated using the standard modified tolerance method [10]. In order of importance, other uncertainties included are estimates of higher-order effects evaluated by scale variation and current measurements of the coupling α_s and the top quark mass [15].

TABLE V. LO and NLO cross sections in (fb) for $pp \to W'_R \to t\bar{b}(\bar{t}b)$ at the LHC, $\sqrt{S} = 7$ TeV, where the decay to leptons is not allowed. NLO includes all theoretical uncertainties listed in the text, and is dominated by PDF uncertainties.

Mass (GeV)	σ^t_{LO} (fb)	$\sigma^{\bar{t}}_{\mathrm{LO}}$ (fb)	σ^t_{NLO} (fb)		$\sigma^{\bar{t}}_{\mathrm{NLO}}$ (fb)	
500	29 300	13 200	37 600	$^{+1900}_{-2400}$	17 100	$^{+1390}_{-940}$
750	6340	2400	7810	$^{+550}_{-420}$	3090	$^{+270}_{-250}$
1000	1800	592	2160	$^{+170}_{-200}$	760	$^{+86}_{-81}$
1250	589	174	689	$^{+53}_{-71}$	225	$^{+29}_{-29}$
1500	209	57.2	237	$^{+26}_{-27}$	75.1	$^{+11.7}_{-10.7}$
1750	78.2	20.4	86.5	$^{+10.1}_{-11.5}$	27.4	$^{+5.1}_{-4.3}$
2000	30.2	7.80	32.7	$^{+4.5}_{-4.8}$	10.9	$^{+2.2}_{-2.0}$
2250	12.1	3.18	12.9	$^{+2.2}_{-1.9}$	4.57	$^{+1.03}_{-0.90}$
2500	5.07	1.40	5.47	$^{+1.01}_{-0.94}$	2.06	$^{+0.49}_{-0.42}$
2750	2.28	0.68	2.55	$^{+0.49}_{-0.39}$	1.01	$^{+0.23}_{-0.19}$
3000	1.13	0.36	1.34	$^{+0.23}_{-0.18}$	0.55	$^{+0.11}_{-0.09}$
3250	0.63	0.22	0.80	$^{+0.11}_{-0.09}$	0.33	$^{+0.05}_{-0.05}$
3500	0.40	0.14	0.52	$^{+0.06}_{-0.05}$	0.21	$^{+0.03}_{-0.02}$

TABLE VI. LO and NLO cross sections in (fb) for $pp \to W'_L \to t\bar{b}(\bar{t}b)$ at the LHC, $\sqrt{S} = 7$ TeV, where the decay to leptons is allowed, but no interference is included (see text). NLO includes all theoretical uncertainties listed in the text and is dominated by PDF uncertainties.

Mass (GeV)	σ^t_{LO} (fb)	$\sigma^{\bar{t}}_{\mathrm{LO}}$ (fb)	σ^t_{NLO} (fb)		$\sigma^{\bar{t}}_{\mathrm{NLO}}$ (fb)	
500	21 500	9700	27 800	$^{+1600}_{-1100}$	12 800	$^{+800}_{-800}$
750	4720	1790	5870	$^{+410}_{-320}$	2330	$^{+200}_{-190}$
1000	1350	445	1630	$^{+110}_{-140}$	575	$^{+74}_{-54}$
1250	444	132	522	$^{+46}_{-46}$	172	$^{+23}_{-20}$
1500	159	43.9	182	$^{+20}_{-19}$	58.2	$^{+8.8}_{-8.3}$
1750	60.1	15.9	67.4	$^{+7.3}_{-8.6}$	21.6	$^{+4.0}_{-3.3}$
2000	23.6	6.23	26.0	$^{+3.4}_{-3.8}$	8.71	$^{+1.68}_{-1.59}$
2250	9.70	2.62	10.6	$^{+1.7}_{-1.6}$	3.77	$^{+0.78}_{-0.74}$
2500	4.21	1.20	4.67	$^{+0.75}_{-0.75}$	1.76	$^{+0.378}_{-0.33}$
2750	1.98	0.60	2.27	$^{+0.38}_{-0.32}$	0.90	$^{+0.17}_{-0.17}$
3000	1.03	0.34	1.25	$^{+0.20}_{-0.14}$	0.50	$^{+0.09}_{-0.07}$
3250	0.60	0.21	0.77	$^{+0.09}_{-0.08}$	0.31	$^{+0.05}_{-0.04}$
3500	0.39	0.14	0.51	$^{+0.05}_{-0.04}$	0.21	$^{+0.02}_{-0.02}$

TABLE VII. LO and NLO cross sections in (fb) for $pp \to W_R' \to t\bar{b}(\bar{t}b)$ at the LHC, $\sqrt{S} = 8$ TeV, where the decay to leptons is not allowed. NLO includes all theoretical uncertainties listed in the text and is dominated by PDF uncertainties.

Mass (GeV)	$\sigma^t_{\rm LO}$ (fb)	$\sigma^{\bar{t}}_{\rm LO}$ (fb)	$\sigma^t_{\rm NLO}$ (fb)		$\sigma^{\bar{t}}_{\rm NLO}$ (fb)	
500	36 800	17 400	47 300	$^{+2300}_{-2800}$	22 500	$^{+2000}_{-1200}$
750	8370	3370	10 400	$^{+740}_{-500}$	4300	$^{+470}_{-210}$
1000	2520	888	3080	$^{+190}_{-293}$	1130	$^{+140}_{-97}$
1250	888	280	1050	$^{+74}_{-97}$	359	$^{+44}_{-36}$
1500	342	99.0	396	$^{+36}_{-44}$	128	$^{+19}_{-16}$
1750	140	38.0	157	$^{+17}_{-16}$	50.0	$^{+7.7}_{-7.6}$
2000	59.0	15.5	65.1	$^{+8.0}_{-8.1}$	20.8	$^{+3.8}_{-3.4}$
2250	25.7	6.68	27.8	$^{+3.9}_{-4.1}$	9.24	$^{+1.86}_{-1.68}$
2500	11.5	3.03	12.3	$^{+2.0}_{-1.8}$	4.32	$^{+0.90}_{-0.86}$
2750	5.31	1.46	5.69	$^{+1.06}_{-0.88}$	2.13	$^{+0.46}_{-0.44}$
3000	2.58	0.75	2.83	$^{+0.52}_{-0.46}$	1.11	$^{+0.24}_{-0.22}$
3250	1.34	0.42	1.54	$^{+0.26}_{-0.24}$	0.62	$^{+0.13}_{-0.11}$
3500	0.76	0.26	0.92	$^{+0.14}_{-0.11}$	0.38	$^{+0.06}_{-0.06}$

TABLE VIII. LO and NLO cross sections in (fb) for $pp \to W_L' \to t\bar{b}(\bar{t}b)$ at the LHC, $\sqrt{S} = 8$ TeV, where the decay to leptons is allowed, but no interference is included (see text). NLO includes all theoretical uncertainties listed in the text and is dominated by PDF uncertainties.

Mass (GeV)	$\sigma^t_{\rm LO}$ (fb)	$\sigma^{\bar{t}}_{\rm LO}$ (fb)	$\sigma^t_{\rm NLO}$ (fb)		$\sigma^{\bar{t}}_{\rm NLO}$ (fb)	
500	27 000	12 800	35 300	$^{+1300}_{-2300}$	16 800	$^{+910}_{-1200}$
750	6230	2510	7780	$^{+600}_{-380}$	3260	$^{+230}_{-290}$
1000	1890	667	2320	$^{+170}_{-200}$	860	$^{+96}_{-78}$
1250	668	212	800	$^{+52}_{-79}$	273	$^{+37}_{-26}$
1500	259	75.5	302	$^{+29}_{-30}$	98.0	$^{+16.2}_{-10.9}$
1750	106	29.3	122	$^{+11}_{-14}$	38.8	$^{+6.1}_{-5.6}$
2000	45.5	12.2	50.9	$^{+5.7}_{-6.5}$	16.5	$^{+2.7}_{-2.8}$
2250	20.1	5.34	22.1	$^{+3.0}_{-2.9}$	7.41	$^{+1.45}_{-1.26}$
2500	9.17	2.49	10.0	$^{+1.5}_{-1.5}$	3.55	$^{+0.71}_{-0.66}$
2750	4.37	1.24	4.79	$^{+0.81}_{-0.67}$	1.80	$^{+0.38}_{-0.33}$
3000	2.20	0.66	2.48	$^{+0.41}_{-0.35}$	0.98	$^{+0.19}_{-0.18}$
3250	1.19	0.38	1.40	$^{+0.21}_{-0.20}$	0.57	$^{+0.11}_{-0.09}$
3500	0.70	0.24	0.86	$^{+0.12}_{-0.09}$	0.36	$^{+0.05}_{-0.05}$

[1] A. Datta, P. J. O'Donnell, Z. H. Lin, X. Zhang, and T. Huang, Phys. Lett. B **483**, 203 (2000).
[2] J. C. Pati and A. Salam, Phys. Rev. D **10**, 275 (1974).
[3] R. N. Mohapatra and J. C. Pati, Phys. Rev. D **11**, 566 (1975).
[4] R. N. Mohapatra and J. C. Pati, Phys. Rev. D **11**, 2558 (1975).
[5] G. Senjanovic and R. N. Mohapatra, Phys. Rev. D **12**, 1502 (1975).
[6] R. S. Chivukula, E. H. Simmons, and J. Terning, Phys. Rev. D **53**, 5258 (1996).
[7] D. E. Groom *et al.* (Particle Data Group Collaboration), Eur. Phys. J. C **15**, 1 (2000).
[8] Y. Mimura and S. Nandi, Phys. Lett. B **538**, 406 (2002).
[9] M. Cvetic and J. C. Pati, Phys. Lett. **135B**, 57 (1984).
[10] Z. Sullivan, Phys. Rev. D **66**, 075 011 (2002).
[11] D. Acosta *et al.* (CDF Collaboration), Phys. Rev. Lett. **90**, 081 802 (2003).
[12] T. Aaltonen *et al.* (CDF Collaboration), Phys. Rev. Lett. **103**, 041 801 (2009).
[13] V. M. Abazov *et al.* (D0 Collaboration), Phys. Lett. B **641**, 423 (2006).
[14] V. M. Abazov *et al.* (D0 Collaboration), Phys. Lett. B **699**, 145 (2011).
[15] J. Beringer *et al.* (Particle Data Group Collaboration), Phys. Rev. D **86**, 010 001 (2012).
[16] G. Aad *et al.* (ATLAS Collaboration), Phys. Rev. Lett. **109**, 081 801 (2012).
[17] S. Chatrchyan *et al.* (CMS Collaboration), arXiv:1208.0956.
[18] Z. Sullivan, in *Proceedings of the XXXVIIIth Rencontres de Moriond: QCD and High Energy Hadronic Interactions, Les Arcs, Savoie, France, 2003*, edited by É. Augé and J. T. T. Vân (Thê Giói Publishers, Hanoi, 2003), p. 379.
[19] Y. Zhou and Z. Sullivan (unpublished).
[20] J. Alwall, P. Demin, S. de Visscher, R. Frederix, M. Herquet, F. Maltoni, T. Plehn, D. L. Rainwater, and T. Stelzer, J. High Energy Phys. 09 (2007) 028.
[21] T. Sjostrand, S. Mrenna, and P. Z. Skands, J. High Energy Phys. 05 (2006) 026.
[22] J. Conway *et al.*, http://www.physics.ucdavis.edu/conway/research/software/pgs/pgs.html.
[23] J. M. Campbell and R. K. Ellis, Nucl. Phys. B, Proc. Suppl. **205–206**, 10 (2010).
[24] P. M. Nadolsky, H.-L. Lai, Q.-H. Cao, J. Huston, J. Pumplin, D. Stump, W.-K. Tung, and C.-P. Yuan, Phys. Rev. D **78**, 013 004 (2008).
[25] Z. Sullivan, http://www.hep.anl.gov/zack/ZTOP/ZTOP.html.
[26] E. Boos, V. Bunichev, L. Dudko, and M. Perfilov, Phys. Lett. B **655**, 245 (2007).
[27] G. Aad *et al.* (ATLAS Collaboration), arXiv:0901.0512.
[28] S. Chatrchyan *et al.* (CMS Collaboration), Phys. Lett. B **716**, 30 (2012).
[29] G. Aad *et al.* (ATLAS Collaboration), Phys. Lett. B **716**, 1 (2012).